

Facile Synthesized NiCo₂O₄ Nanoparticles as Electrode Material for Supercapacitors

Tianfu Huang^{1,2,*}, Bo Liu², Pei Yang², Zehai Qiu^{1,2}, Zhibiao Hu^{1,2}

¹Fujian Provincial Key Laboratory of Clean Energy Materials, Longyan University, Fujian Longyan, 364012, China

²College of Chemistry & Materials Science, Longyan University, Fujian Longyan, 364012, China

*E-mail: hhtff@126.com

Received: 24 January 2018 / Accepted: 9 March 2018 / Published: 10 May 2018

NiCo₂O₄ nanoparticles were successfully synthesized by a simple, fast and cost effective sucrose-assisted combustion route, and followed by calcination treatment. When NiCo₂O₄ nanoparticles were used as electrode materials for supercapacitors, the NiCo₂O₄ electrodes delivered a high specific capacitance of 429.6 F g⁻¹ at a current density of 1 A g⁻¹, remarkable capacitance retention rate of 74.30% at current density of 16 A g⁻¹ compared with 1 A g⁻¹, and 88.54% retention after 4000 cycles. The as-prepared NiCo₂O₄ nanoparticles hold promise for practical application of high-performance supercapacitors due to the facile and low cost effective synthesized method and superior electrochemical performances.

Keywords: Nanoparticles; Cobalt acid nickel; Supercapacitor

1. INTRODUCTION

Nowadays, the search for high-performance electrochemical energy storage devices have drawn significant attention due to the fossil-fuel crisis and increasing demand for renewable energy in the modern society [1]. As a kind of energy storage device, supercapacitors have its unique properties, such as fast charge-discharge rate, high power density and stable cycling performance. Generally, there are two type of storage energy mechanism for supercapacitors: one is fast surface redox reactions (pseudocapacitors); the other is ion adsorption (electrical double-layer capacitors, EDLCs) [2]. As is well known, the electrochemical performance of supercapacitors is largely determined by the properties of electrode materials. So, it is imperative to develop novel electrode materials with superior electrochemical performance but at low cost for the development of supercapacitors.

Potentially, pseudocapacitors can provide much higher capacitance values than EDLCs through Faradic reaction [3]. Up to now, transition metal oxides with variable valence have been widely used in pseudocapacitors, such as MnO_2 [4], Co_3O_4 [5], MnCo_2O_4 [6, 7], NiCo_2S_4 [8, 9], etc. Many researchers focus on binary metal oxides. According to relevant literature [10, 11], binary metal oxides may possess a higher electrochemical activity and higher electronic conductivity than those of monometallic oxides. NiCo_2O_4 with spinel crystal structure is one of the typical representatives of binary transition metal oxides. So there are a lot of relevant reports of supercapacitors about NiCo_2O_4 . For example, Q. Zheng [12] has reported that hierarchical porous NiCo_2O_4 films composed of nanowalls on nickel foam are synthesized via a facile hydrothermal method, the as-prepared NiCo_2O_4 films display a high capacity of 130 mAhg^{-1} at 2 A g^{-1} and are 97% capacity maintained after 2000 cycles. X. Ji [13] has reported that NiCo_2O_4 nanorods are synthesized via solid state reactions at room temperature coupled with a simple post annealing treatment, the as-prepared NiCo_2O_4 nanorods manifest a high specific capacitance of 565 F g^{-1} at a current density of 1 A g^{-1} with superior rate capability and good cycling stability. Y. Zhu [14] reported that the 3D NiCo_2O_4 displays high specific capacitance of 931 F g^{-1} at 3 A g^{-1} , remarkable capacity retention rate of 85.2% and 72.5% at 20 and 50 A g^{-1} compared with 2 A g^{-1} and superior cycling stability of 125.2% of initial capacity retention over 1000 cycles at 3 A g^{-1} .

There are many advantages for sucrose-assisted combustion synthesis [15]. In this article, we demonstrate the design and synthesis of NiCo_2O_4 nanoparticles via a sucrose-assisted combustion route followed by calcination treatment. To the best of our knowledge, the sucrose-assisted combustion method has rarely been reported to synthesize NiCo_2O_4 nanoparticles. When used as an electrode for supercapacitor, the NiCo_2O_4 nanoparticles exhibit a high specific capacitance, remarkable capacitance retention rate and excellent cycling stability, suggesting their promising application in supercapacitors.

2. EXPERIMENTAL

2.1. Synthesis of the NiCo_2O_4 nanoparticles

All the materials were analytical reagent grade and used as received without any further purification in the experiments.

In a typical procedure, First, 1.164 g $\text{Co}(\text{NO}_3)_2 \cdot 6\text{H}_2\text{O}$ (4m mol) and 0.582 g $\text{Ni}(\text{NO}_3)_2 \cdot 6\text{H}_2\text{O}$ (2m mol) were dissolved in 6 mL of deionized water in the beaker. Second, 0.684g $\text{C}_{12}\text{H}_{22}\text{O}_{11}$ (2m mol) was added and were dissolved to form a mixed solution. Third, the beaker was put into furnace at $140 \text{ }^\circ\text{C}$ for 1 h. The loose powders of NiCo_2O_4 were obtained after complete combustion. At last, they were calcined under air atmosphere at $350 \text{ }^\circ\text{C}$ for 6 h, resulting in NiCo_2O_4 nanoparticles. Also, NiO and Co_3O_4 were prepared via the same method.

2.2. Structure characterization

The morphology of NiCo_2O_4 was characterized by FE-SEM. The crystal structure of NiCo_2O_4 was examined by XRD. The Brunauer-Emmett-Teller (BET) specific surface area was obtained from the N_2 adsorption/desorption isotherm recorded at 77K.

2.3. Electrochemical measurements

The working electrodes were prepared according to our previous work [11]. The working electrode was prepared by mixing the PTFE binder, carbon black and the electroactive material (NiCo_2O_4 nanoparticles) in a weight ratio of 5:10:85. A few drops of ethanol were added to the mixture to achieve a homogeneous slurry. The slurry was pressed onto the nickel foam under 12 MPa, and dried at 60°C for 6 h, which is named as NiCo_2O_4 electrode.

Electrochemical measurements were performed in a solution of 6 M KOH aqueous electrolyte using a three-electrode cell. NiCo_2O_4 electrode was used to make working electrodes. Hg/HgO electrodes and platinum foil were used as reference and counter electrodes, respectively. The comprehensive electrochemical performances were evaluated by characterizing their electrochemical impedance spectroscopy (EIS), galvanostatic charge/discharge (GCD) and cyclic voltammetry (CV). All the measurements were performed at room temperature.

3. RESULTS AND DISCUSSION

3.1. Formation mechanism of the NiCo_2O_4

The typical process is based on the mixing of metal nitrates and an organic fuel. There are citric acid, sucrose and urea, etc. for common organic fuels. Among them, sucrose is cheap, available at industrial scale, nontoxic, and easy to store and manipulate at low temperatures. So, the sucrose-assisted combustion synthesis is environmentally friendly and green method.

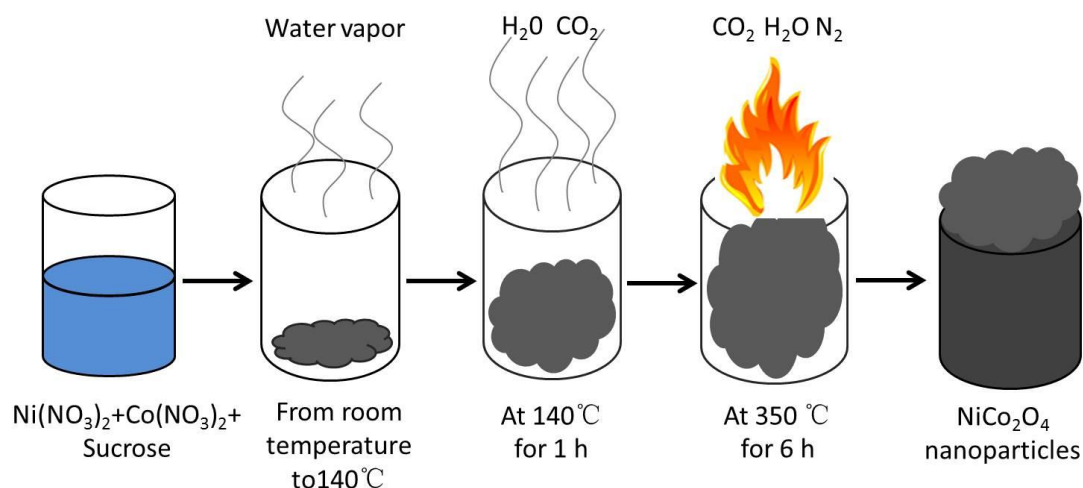
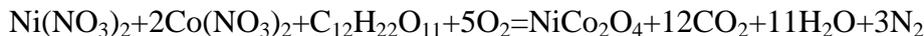


Figure 1. Schematic representation of the sucrose-assisted combustion synthesis of NiCo_2O_4 nanoparticles

Fig.1 illustrates a representative fabrication process of the NiCo_2O_4 nanoparticles. During heating process from room temperature to 140°C , the homogeneous mixed solution produced a large amount of water vapor. And, when the obtained mixed solution in the 50 mL of beaker was heated in the oven at 140°C for 1 h, it changed into sol, sticky gel, solid gel, etc. Once solid gel was obtained, gel

combustion process can occur. The violence combustion could result in the formation of carbonaceous black colored fluffy mass by emitting H_2O , CO_2 and N_2 gases. The loose powders of NiCo_2O_4 were obtained after complete combustion. These powders were then called as-prepared sucrose precursors. At last, the precursors were calcined under air atmosphere at 350°C for 6 h, resulting in NiCo_2O_4 nanoparticles. The typical total combustion reaction can be written as follows:



The sucrose-assisted combustion synthesis is environmentally friendly and green method. According to the relevant literatures, the sucrose-assisted combustion synthesis is widely used to synthesize BiFeO_3 nanopowders [16, 17], $\text{MgO-Y}_2\text{O}_3$ Nanocomposites [18], NiFe_2O_4 [19], etc.

3.2. Structure and surface morphology characterization

The crystal structure and phase information were obtained by XRD measurements. The crystalline size D_c was calculated by using the Scherrer equation [20, 21], $D_c = 0.89\lambda / (\beta \cos\theta)$, where, θ is the Bragg angel of the diffraction peak, β is the full width at half-maximum corrected for instrumental broadening, and λ is the corrected wavelength of the X-radiation. Fig.2a shows the X-ray diffraction patterns of NiCo_2O_4 calcined at 350°C . Obviously, it can be seen that the target compounds are well-crystallized, which can be discerned from the diffraction peaks.

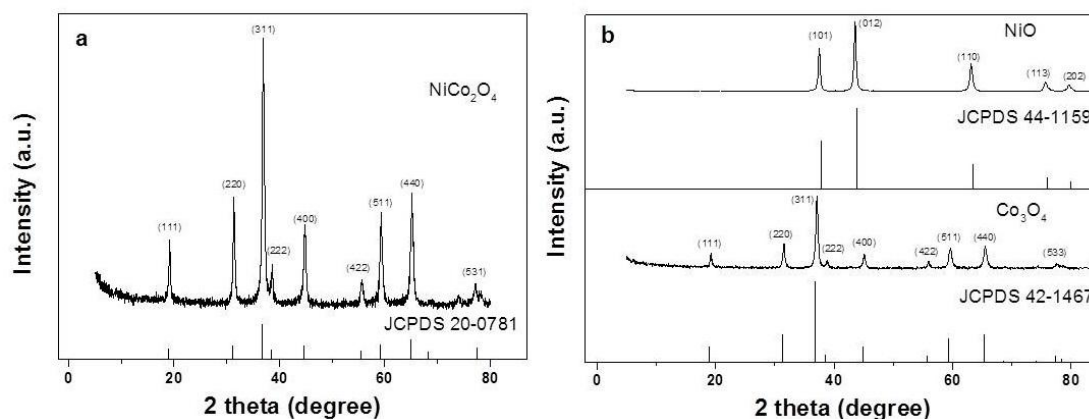


Figure 2. (a)The X-ray diffraction patterns of NiCo_2O_4 calcined at 350°C ; (b)The X-ray diffraction patterns of NiO and Co_3O_4 calcined at 350°C

The sharp diffraction peaks at 2θ of 19.187, 31.369, 36.948, 38.631, 44.870, 55.730, 59.302, 65.208 and 77.238 can be indexed as (111), (220), (311), (222), (400), (422), (511), (440) and (531) crystal planes. The resultant diffraction peaks corroborate well with the standard pattern of spinel NiCo_2O_4 (JCPDS 20-0781, cubic crystal system) and no peaks of other phases are detectable. In addition, the crystal lattice parameter ($a=b=c=8.108 \text{ \AA}$) calculated from the XRD results of sample prepared at 350°C is highly similar with the standard data ($a=b=c=8.110 \text{ \AA}$) of NiCo_2O_4 [12]. It also can be calculated that the average grain size of NiCo_2O_4 by applying Scherrer's equation [20, 21]. The mean grain size of as prepared NiCo_2O_4 is 25.470 nm. In addition, NiO and Co_3O_4 were successfully

prepared via the same method. As shown in Fig.2b, the resultant diffraction peaks corroborate well with the standard pattern of NiO (JCPDS 44-1159) and Co₃O₄ (JCPDS 42-1467).

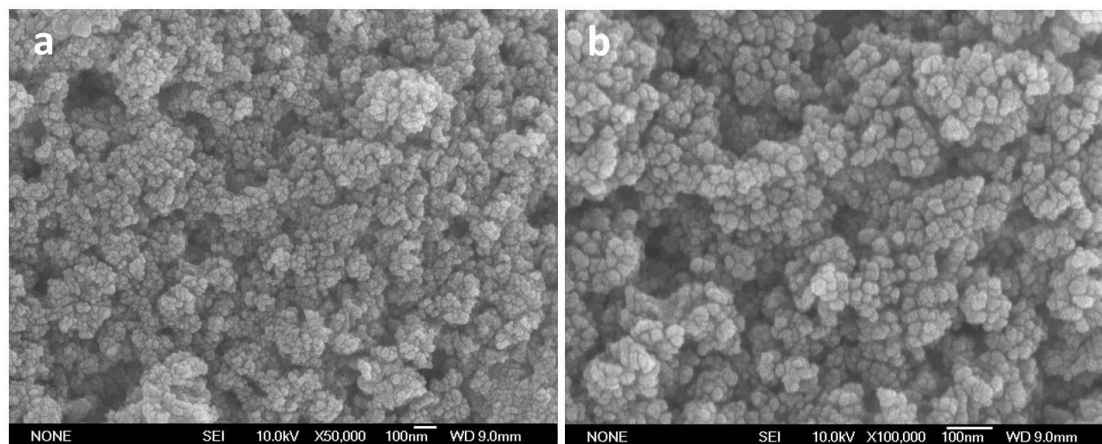


Figure 3. The SEM (a-b) images of NiCo₂O₄ nanoparticles

Detailed structural and morphological information was further investigated by FE-SEM. Fig.3 shows FESEM images of the NiCo₂O₄ at 50000 and 100000 magnifications. Interestingly, it can be clearly observed that the as-synthesized NiCo₂O₄ sample comprises highly uniform and well defined small particles. And, the as-prepared NiCo₂O₄ possess average particles size in the range of ~22-28 nm, as shown in Fig.3, which is consistent with the calculated results by applying Scherrer’s equation. The unique spherical shaped particles may be due to the sucrose-assisted combustion. During this procedure, they emitted H₂O, CO₂ and N₂ gases when the reactants were decomposed.

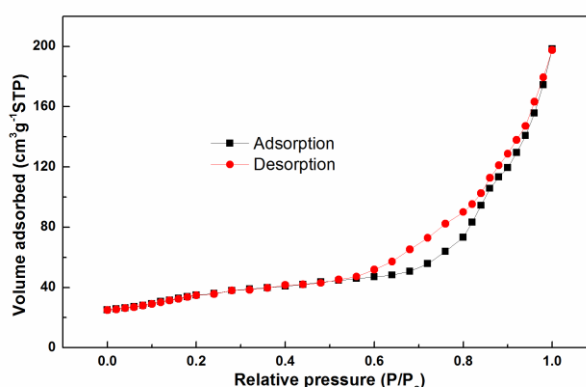


Figure 4. Nitrogen adsorption and desorption isotherms of NiCo₂O₄

The surface area was investigated using nitrogen adsorption and desorption isotherms. Fig.4 displays the nitrogen adsorption/desorption isotherm of the obtained NiCo₂O₄, and its curve belongs to a type-IV isotherm with a H3 hysteresis loop in the relative pressure range of 0.56-1.0. BET specific surface area of the obtained NiCo₂O₄ sample is calculated to be as high as 162.59 m² g⁻¹ according to the nitrogen adsorption-desorption isotherm. It is well known that the larger specific surface area of

material is, the richer electroactive sites of materials for Faraday reaction are. The as-prepared NiCo₂O₄ was highly uniform and well defined small particles with a specific surface area of 162.59 m² g⁻¹, and this can promote supercapacitor performance effectively. Therefore, the large specific surface area renders the NiCo₂O₄ nanoparticles more suitable for supercapacitor application.

3.3. Electrochemical measurements

Cyclic voltammetry (CV) has been performed to evaluate the electrochemical properties and quantify the specific capacitance of as-prepared NiCo₂O₄ electrode. Fig.5a presents the cyclic voltammetry (CV) curves of the NiCo₂O₄ electrode at different scan rates ranging from 5 to 50 mV s⁻¹. Interestingly, it is found that the electrodes exhibit a pair of redox peak and different shapes (not rectangular shape) of charge-discharge curves, which clearly indicate the pseudo-capacitive characteristics derived from the redox Faradaic reaction. The redox reactions in an alkaline electrolyte are based on the following equations [22]:

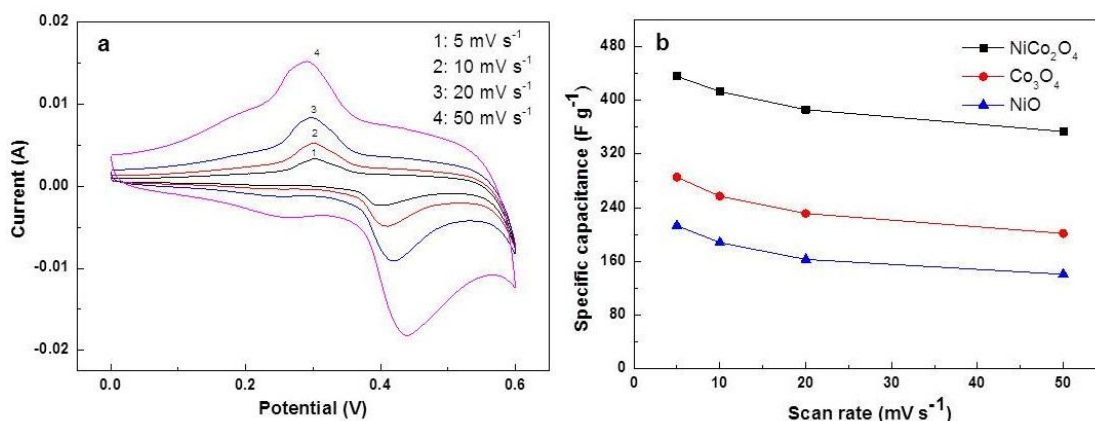
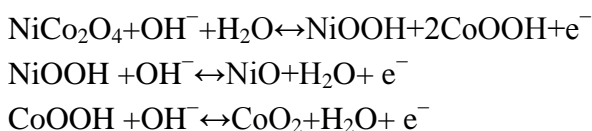


Figure 5. (a) CV curves of NiCo₂O₄ at various scan rates ranging from 5 to 50 mV s⁻¹; (b) calculated specific capacitance of the NiCo₂O₄, Co₃O₄ and NiO samples as a function of the scan rate

From the Fig.5a, we also find that the anodic and cathodic peaks shift to higher and lower potentials as the scan rates increase from 5 to 50 mV s⁻¹, respectively. The NiCo₂O₄ electrodes are beneficial to fast redox reactions and thus high-power characteristic can be expected. The average specific capacitance can be calculated by the following formula:

$$C = \frac{1}{s \cdot m \cdot \Delta V} \int_{V_2}^{V_1 + \Delta V} I(V) dV$$

where I (A) is the current, m (g) is the mass of the active material in the electrode, s (V s⁻¹) is the scan rate, V is the voltage in the CV curve. According to the CV curves, the average specific

capacitance of NiCo_2O_4 was calculated to be 435.7, 413.05, 386.07 and 353.5 F g^{-1} at the scan rates of 5, 10, 20 and 50 mV s^{-1} , respectively, which are much higher than the specific capacitances of Co_3O_4 and NiO , as shown in Fig.5b. The results coincide with the relevant reporting literature [10, 11].

From the Fig.5b, we also find that the specific capacitances of NiCo_2O_4 , Co_3O_4 and NiO decrease as the scan rates increase. In fact, at low scan rates, the ions of the electrolyte have enough time to enter into active material. Therefore, increasing the scan rate caused a decrease in the total specific capacitance. Remarkably, about 81.13% of the specific capacitance of NiCo_2O_4 can be retained for a 10-time increase in scan rate. However, about 70.65% of the specific capacitance of Co_3O_4 can be retained, and about 65.99% of the specific capacitance of NiO can be retained.

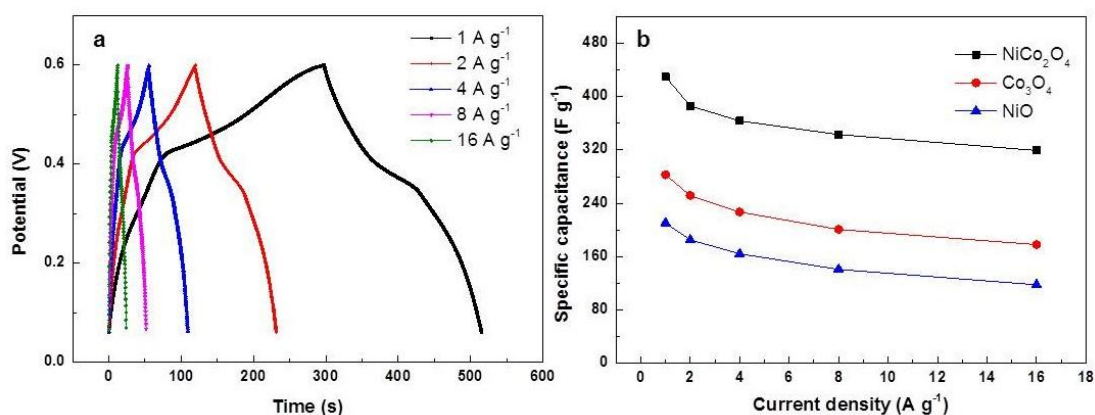


Figure 6. (a) galvanostatic charge-discharge curves of NiCo_2O_4 at various current densities ranging from 1 to 16 A g^{-1} ; (b) calculated specific capacitance of the NiCo_2O_4 , Co_3O_4 and NiO samples as a function of the current density

To further evaluate the comprehensive electrochemical performances, galvanostatic charge-discharge (GCD) measurement was also tested with the currents ranging from 1 to 16 A g^{-1} . Fig.6a shows the constant current charge-discharge profiles at different current densities. Obviously, it can be observed that symmetric, indicating the high columbic efficiency, reversible behavior, and ideal capacitor performance under various current densities. The nonlinear charge/discharge profiles further verified the pseudo-capacitance behavior.

The specific capacitance is calculated from discharge time using the following formula:

$$C_m = \frac{C}{m} = \frac{I \times \Delta t}{\Delta V \times m}$$

where, $C_m (\text{F g}^{-1})$ is the specific capacitance, $I (\text{A})$ is discharge current, $\Delta t (\text{s})$ is the discharging time, $\Delta V (\text{V})$ represents the potential drop during discharge process, and $m (\text{g})$ is the mass of the active material in the electrode. The calculated specific capacitance as a function of the discharge current density is plotted in Fig.6b. The specific capacitances of NiCo_2O_4 are 429.6, 386.1, 363.6, 343.2 and 319.2 F g^{-1} at different current densities of 1, 2, 4, 8 and 16 A g^{-1} , respectively. The specific capacitance values of NiCo_2O_4 , Co_3O_4 and NiO are also compared in Fig.6b. It depicts that the specific capacitance of NiCo_2O_4 electrode is obviously much higher than those of the Co_3O_4 and NiO

electrodes. The phenomenon may be attributed the binary metal oxides, which possess a higher electronic conductivity and higher electrochemical activity than those of monometallic oxides.

In practice, the ability to discharge at high rates is also crucial in capacitors. The discharge capacitances of NiCo_2O_4 , Co_3O_4 and NiO at 16 A g^{-1} keep 74.30%, 63.01% and 56.02% of those discharged at 1 A g^{-1} , respectively. Obviously, NiCo_2O_4 electrode exhibits good rate capability. So the as-prepared NiCo_2O_4 nanoparticles hold promise for practical application of high-performance supercapacitors.

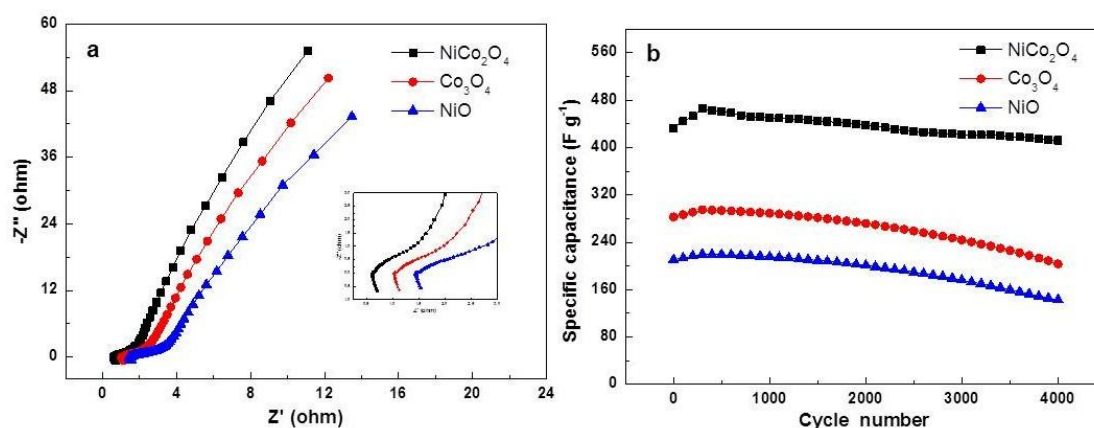


Figure 7. (a) The EIS curves of NiCo_2O_4 , Co_3O_4 and NiO ; (b) the electrochemical stability test curves of NiCo_2O_4 , Co_3O_4 and NiO

The EIS analysis is an important method for the supercapacitive performance investigation. Fig.7a shows the EIS in the form of plots of NiCo_2O_4 , Co_3O_4 and NiO , where Z' and Z'' are the real and imaginary parts of the impedance. Obviously, all the impedance plots were similar, being composed of one semicircle component at high frequency followed by a linear component at the low frequency. As was shown in Fig.7a, the electrode resistances of NiCo_2O_4 , Co_3O_4 and NiO electrodes, obtained from the intercept of the plots on real axis, are about 0.48, 0.63 and 0.85 Ω . The pseudo charge transfer resistance (R_{ct}) depends on the semicircle. The calculated R_{ct} of the NiCo_2O_4 , Co_3O_4 and NiO are 0.26, 0.36 and 0.47 Ω according to the diameter of the semicircle. In the low frequency range, the Warburg tail is expected to occur at 45° , corresponding to the capacitor's diffusive resistance of the electrolyte. Obviously NiCo_2O_4 shows the lower Warburg impedance compared with Co_3O_4 and NiO .

The cycling stability is a prerequisite requirement for electrode materials. The cycling stability of NiCo_2O_4 , Co_3O_4 and NiO were performed by charge-discharge test at a current density of 1 A g^{-1} . As shown in Fig.7b, the specific capacitance of electrode has a gradual increase in a few hundred cycles, and can reach a maximum value. Then it decreases slightly compared with the maximum value. The penetration of electrolyte ions and the gradual activation of the active materials may be responsible for the increase of the specific capacitance in the first several hundred cycles. The specific capacitance of NiCo_2O_4 can reach a maximum of 465.68 F g^{-1} . But the specific capacitance of NiCo_2O_4 still remained 412.29 F g^{-1} , and degraded only by 11.46% after 4000 cycles of charge-

discharge. The phenomenon coincides with the reporting literatures [16]. In the control experiment, Co_3O_4 and NiO also displayed a relatively small increase in specific capacitance after several charge and discharge cycles, the specific capacitance of Co_3O_4 and NiO can reach a maximum of 294.99 and 219.88 F g^{-1} respectively. But the specific capacitance of Co_3O_4 and NiO only remained 203.54 and 143.02 F g^{-1} , and degraded sharply by 31.00% and 34.96% after 4000 cycles of charge-discharge, respectively. Therefore, cycling stability of NiCo_2O_4 is much better than those of Co_3O_4 and NiO .

Table 1. Comparison of the electrochemical performances of the NiCo_2O_4 prepared in present work and other reports in previous works.

Sample	Specific capacitance	Rate capacitance	Cycle stability	Reference
Porous NiCo_2O_4 flowerlike nanostructure	658 F g^{-1} at 1A g^{-1}	78% from 1 to 20 A g^{-1}	90% retention after 10000 cycles	[23]
Porous hexagonal NiCo_2O_4 nanoplates	294 F g^{-1} at 1A g^{-1}	/	89.8% retention after 2200 cycles	[24]
Urchin-like NiCo_2O_4 sub-microspheres	296 F g^{-1} at 1A g^{-1}	72.6% from 1 to 5 A g^{-1}	/	[25]
NiCo_2O_4 nanoneedle arrays	3.12 F cm^{-2} at 1.11 mA cm^{-2}	18.9% from 1.11 to 22.24 mA cm^{-2}	94.74% retention after 2000 cycles	[26]
NiCo_2O_4 nanoparticles	429.6 F g^{-1} at 1A g^{-1}	74.30% from 1 to 16 A g^{-1}	88.54% retention after 4000 cycles	This work

It is necessary to make comparison the NiCo_2O_4 nanoparticles electrode material with similar electrode materials for supercapacitors that were described in literatures. Tab.1 is comparison of the electrochemical performances of the NiCo_2O_4 prepared in present work and other reports in previous works [23-26]. As is shown in Tab.1, the specific capacitance of porous hexagonal NiCo_2O_4 nanoplates is 294 F g^{-1} at 1A g^{-1} , the specific capacitance of urchin-like NiCo_2O_4 sub-microspheres is 296 F g^{-1} at 1A g^{-1} . But, the specific capacitance of NiCo_2O_4 nanoparticles is 429.6 F g^{-1} at 1A g^{-1} . Moreover, the rate capacitance of NiCo_2O_4 nanoparticles is 74.30% from 1 to 16 A g^{-1} , the cycle stability of NiCo_2O_4 nanoparticles is 88.54% retention after 4000 cycles. Therefore, the as-prepared NiCo_2O_4 electrode displays excellent comprehensive electrochemical properties by comparison.

4. CONCLUSIONS

In summary, we have successfully synthesized NiCo_2O_4 nanoparticles by a simple, fast and cost effective sucrose-assisted combustion route followed by calcination treatment, and the capacitive behavior was successfully investigated in an alkaline electrolyte. The as-prepared NiCo_2O_4 electrode displays a high specific capacitance of 429.6 F g^{-1} at a current density of 1 A g^{-1} , remarkable

capacitance retention rate of 74.30% at current density of 16 A g⁻¹ compared with 1 A g⁻¹, and excellent cycle stability (only 11.46% loss after 4000 cycles). It should not be ignored that the highly uniform and well defined small nanoparticles played very important roles in improving specific capacitance, power performance and cycle stability. Meanwhile, the present work displays the design of next generation of low-cost and ultrahigh performance binary metal oxide electrode materials prepared by facile method. Therefore, the as-prepared NiCo₂O₄ nanoparticles hold promise for practical application of high-performance supercapacitors.

ACKNOWLEDGEMENTS

This work was financially supported by the National Training Programs of Innovation and Entrepreneurship for Undergraduates (201611312010), the provincial level key subject, the young and middle-aged project of education department of Fujian Province (JAT170566).

References

1. X. Zheng, H. Wang, C. Wang, Z. Deng, L. Chen, Y. Li, T. Hasan, B. L. Su, *Nano Energy*, 22 (2016) 269.
2. J. Chen, Y. Huang, C. Li, X. Chen, X. Zhang, *Appl Surf Sci.*, 360 (2016) 534.
3. K. Adib, M. R. Nasrabadi, Z. Rezvani, S. M. Pourmortazavi, F. Ahmadi, H. R. Naderi, M. R. Ganjali, *J Mater Sci: Mater Electron.*, 27 (2016) 4541.
4. N. Li, X. Zhu, C. Zhang, L. Lai, R. Jiang, J. Zhu, *J Alloy Compd.*, 692 (2017) 26.
5. S. K. Meher, G. R. Rao, *J. Phys. Chem. C.*, 115 (2011) 15646.
6. K. N. Hui, K. S. Hui, Z. Tang, V. V. Jadhav, Q. X. Xia, *J. Power Sources*, 330 (2016) 195.
7. H. Che, A. Liu, J. Mu, C. Wu, X. Zhang, *Ceram Int.*, 42 (2016) 2416.
8. F. Zhao, W. Huang, Q. Shi, D. Zhou, L. Zhao, H. Zhang, *Mater Lett.*, 186 (2017) 206.
9. L. Hou, R. Bao, Z. Chen, M. Rehan, L. Tong, G. Pang, C. Yuan, *Electrochim. Acta*, 214 (2016) 76.
10. L. B. Kong, C. Lu, M. C. Liu, Y. Luo, L. Kang, X. Li, F. C. Walsh, *Electrochim. Acta*, 115 (2014) 22.
11. T. Huang, C. Zhao, R. Zheng, Y. Zhang, Z. Hu, *Ionics*, 21 (2015) 3109.
12. Q. Zheng, X. Zhang, Y. Shen, *Mater Res Bull.*, 64 (2015) 401.
13. Y. Zhu, X. Pu, W. Song, Z. Wu, Z. Zhou, X. He, F. Lu, M. Jing, B. Tang, X. Ji, *J Alloy Compd.*, 617 (2014) 988.
14. Y. Zhu, Z. Wu, M. Jing, W. Song, H. Hou, X. Yang, Q. Chen, X. Ji, *Electrochim. Acta*, 149 (2014) 144.
15. T. Li, J. Shen, N. Li, M. Ye, *J Alloy Compd.*, 548 (2013) 89.
16. S. Farhadi, M. Zaidi, *J. Mol. Catal. A: Chem.*, 299 (2009) 18.
17. Tie Li, Jianfeng Shen, Na Li, *J Alloy Compd.*, 548 (2013) 89.
18. A. Iyer, J. Garofano, J. Reutenaur, S. Suib, M. Aindow, M. Gell, E. Jordan, *J. Am. Ceram. Soc.*, 96 (2013) 346.
19. M. Gabal, S. Kosa, T. Muttairi, *Ceram Int.*, 40 (2014) 675.
20. P. Scherrer, *Göttinger Nachrichten Gesell.*, 2 (1918) 98.
21. A. L. Patterson, *Phys. Rev.*, 56 (1939) 978.
22. T. Yan, R. Li, Z. Li, Y. Fang, *Electrochim. Acta*, 134 (2014) 384.
23. H. Chen, J. Jiang, L. Zhang, T. Qi, D. Xia, H. Wan, *J. Power Sources*, 248 (2014) 28.
24. J. Pu, J. Wang, X. Jin, F. Cui, E. Sheng, Z. Wang, *Electrochim. Acta*, 106 (2013) 226.

25. T. Wu, J. Li, L. Hou, C. Yuan, L. Yang, X. Zhang, *Electrochim. Acta*, 81 (2012) 172.
26. G. Zhang, H. Wu, H. Hoster, M. Chan-Park, X. Lou, *Energy Environ. Sci.*, 5 (2012) 9453.

© 2018 The Authors. Published by ESG (www.electrochemsci.org). This article is an open access article distributed under the terms and conditions of the Creative Commons Attribution license (<http://creativecommons.org/licenses/by/4.0/>).